International Journal of Bifurcation and Chaos, Vol. 17, No. 10 (2007) 3415–3424

SPECIAL PROPERTIES OF IMAGES AND CORRESPONDING SIGNALS GENERATED BY CHEMICAL REACTIONS DISCRETE CHAOTIC DYNAMICS

V. GONTAR* and O. GRECHKO
International Group for Chaos Studies,
Department of Industrial Engineering and Management,
Ben-Gurion University of the Negev, P. O. Box 653,
Beer Sheva 84105, Israel
**galita@bgu.ac.il*

Received September 29, 2005; Revised August 15, 2006

A system of difference equations derived from chemical reactions discrete chaotic dynamics (DCD) is used to generate different types of images and corresponding discrete time series (signals). Dynamic properties of the generated time series and images are illustrated by partial bifurcation diagrams, partial intermediate bifurcation diagrams and Lyapunov exponents. Examples of images and signals have been presented. Some special relations between images and signals generated by DCD have been established and discussed.

Keywords: Discrete chaotic dynamics; mathematical imaging; time series analyses.

1. Introduction

Mathematical imaging and signal processing based on the exploitation of difference equations is a growing computer science domain [Mandelbrot, 2004; Peitgen *et al.*, 2004]. In this work, we present and discuss some properties of images and signals (discrete time series) generated by the difference equations derived from chemical reactions discrete chaotic dynamics (DCD) [Gontar, 1997].

DCD is a theory exploring the first principles and laws of physics for mathematical modeling of chemical reactions dynamics in discrete time and space. The basic equations of DCD form a system of nonlinear difference equations written for the concrete mechanism of chemical transformations, accomplished with "information exchange". Accordingly, these difference equations could simulate local chemical reactions dynamics in "discrete time" (the discrete analog to the ordinary differential equations of the kinetic mass action law), or distributed chemical reactions dynamics in "discrete time" and "discrete space" (the discrete analog to the partial differential equations of the kinetic mass action law) [Gontar, 1997, 2000, 2004].

The discrete space is represented by a squared lattice, in which each cell is characterized by the constituent concentrations calculated according to the concrete mechanism of the chemical reactions. With DCD, the rates of the chemical reactions taking place in each cell are dependent upon the constituent concentrations in the neighboring cells ("information exchange"). Therefore, the complex discrete time-space-distributed chemical reaction is characterized by the calculated values of constituent concentrations in each cell of the lattice at each moment of "discrete time". We understand discrete time to be the sequence of the states of the system as they evolve from the initial conditions, in accordance with the chemical transformations and the "information exchange".

To visualize the space-distributed evolution of the constituent concentrations on a discrete lattice, their values are encoded by a colored palette. The evolution of the constituent concentrations that takes place in each cell of the lattice is presented as a discrete time series. It will be shown that these discrete time series and corresponding distributions of chemical constituents demonstrate interesting dynamic properties such as self-organization in the form of creative patterns (symmetrical images, spirals, etc.) and coexistence of chaotic and periodic signals within one dynamic system. We intend to demonstrate a strong correlation between the chaotic oscillatory regimes that appear within the individual cells and the global organization of the constituents over the entire lattice in the form of creative patterns (images). To analyze these dynamic properties, partial bifurcation diagrams, partial intermediate bifurcation diagrams and Lyapunov exponents have been calculated [Schuster, 1984].

2. Background

To demonstrate the use of a DCD mathematical model for signal and image generation, we use the following set of difference equations, derived for the particular mechanism of chemical constituents' interactions with "information exchange" [Gontar, 1997]:

$$X_1^{t_q}(R_p,R_s)=\frac{b}{1+\pi_1(X_i^{t_{q-1}}(r\otimes))+\pi_1(X_i^{t_{q-1}}(r\otimes))\pi_2(X_i^{t_{q-1}}(r\otimes))} \tag{1}$$

$$X_2^{t_q}(R_p,R_s)=\frac{b\pi_1(X_i^{t_{q-1}}(r\otimes))}{1+\pi_1(X_i^{t_{q-1}}(r\otimes))+\pi_1(X_i^{t_{q-1}}(r\otimes))\pi_2(X_i^{t_{q-1}}(r\otimes))} \tag{2}$$

$$X_3^{t_q}(R_p,R_s)=\frac{b\pi_1(X_i^{t_{q-1}}(r\otimes))\pi_2(X_i^{t_{q-1}}(r\otimes))}{1+\pi_1(X_i^{t_{q-1}}(r\otimes))+\pi_1(X_i^{t_{q-1}}(r\otimes))\pi_2(X_i^{t_{q-1}}(r\otimes))} \tag{3}$$

$$\pi_1(X_i^{t_{q-1}}(r\otimes))=k_1\exp\left\{-\left[\sum_{i=1}^{3}\alpha_i X_i^{t_{q-1}}(R_p,R_s)+\sum_{i=1}^{3}\beta_i X_i^{t_{q-1}}(r\otimes)\right]\right\} \tag{4}$$

$$\pi_2(X_i^{t_{q-1}}(r\otimes))=k_2\exp\left\{-\left[\sum_{i=1}^{3}\alpha_i X_i^{t_{q-1}}(R_p,R_s)+\sum_{i=1}^{3}\beta_i X_i^{t_{q-1}}(r\otimes)\right]\right\} \tag{5}$$

where $i=1,2,3$; $X_i^{t_q}(R_p,R_s)$ is the concentration of the ith constituent calculated in each cell of the lattice with integer coordinates (R_p,R_s) at the discrete time t_q ($q=1,2,\ldots,Q$, $R_p,R_s=1,2,\ldots,R$); $\pi_l(X_i^{t_{q-1}}(r\otimes))$ are the functions of system's constituents concentrations calculated at discrete time t_{q-1} and of the neighboring concentrations $X_i^{t_{q-1}}(r\otimes)$ of the lth reaction ($l=1,2$); b is the total concentration of the main constituent; k_l - is the rate constant of lth reaction; α_i are the empirical parameters characterizing local "information exchange" between the constituents inside the considered cell; β_i are the empirical parameters characterizing the "information exchange" emanating from the constituents in the eight closest neighboring cells, including the considered cell. Each vector $r\otimes$ contains nine discrete coordinates: $r\otimes=[(R_p-1,R_s-1),(R_p-1,R_s),(R_p-1,R_s+1),(R_p,R_s-1),(R_p,R_s),(R_p,R_s+1),(R_p+1,R_s-1),(R_p+1,R_s),(R_p+1,R_s+1)]$. Therefore, the influences received by the chemical reactions in the particular cell from their neighbors ("information exchange") are formally introduced into Eqs. (1)–(3), by establishing the concrete dependence of $\pi_l(X_i^{t_{q-1}}(r\otimes))$ on the concentrations of $X_i^{t_{q-1}}(r\otimes)$ in Eqs. (4) and (5).

The initial and the boundary conditions are given as:

$$X_1^{t_0}(R_p,R_s)=b,\quad X_2^{t_0}(R_p,R_s)=0,\quad X_3^{t_0}(R_p,R_s)=0,\quad R_p,R_s=1,2,\ldots,R \tag{6}$$

$$X_i^{t_q}(R_p,R_s)=\begin{cases}X_i^{t_q}(R_p,R_s), & 1\le R_p,\ R_s\le R & \text{(inside the lattice)}\\ 0, & R_p,R_s<1;R_p,\ R_s>R & \text{(outside the lattice)}\end{cases} \tag{7}$$

Based on Eqs. (1)–(3), all the concentrations are changing within the interval $0 < X_i^{t_q}(R_p, R_s) < b$. The calculated values of the concentrations within each cell of the considered lattice are represented by colors from the 256-color palette. For Eqs. (1)–(3), the results are three ($i = 1, 2, 3$) sequences (t_q, $q = 1, 2, \ldots, Q$) of the values of the lattice-distributed chemical constituents: $X_1^{t_q}(R_p, R_s)$, $X_2^{t_q}(R_p, R_s)$ and $X_3^{t_q}(R_p, R_s)$ ($R_p, R_s = 1, 2, \ldots, R$).

To account for the changes in constituent concentrations in each cell of the lattice in discrete time, we present these changes as a discrete time series. To illustrate the dynamics of these local time series, we introduce partial (for one chosen parameter) intermediate bifurcation diagrams (PIBDs). PIBDs differ from classic bifurcation diagrams (BDs) in that they are calculated at intermediate dynamic states. While the process should converge to an asymptotic state at $t_q \to 10000$, here we present PIBDs for the 150 states, taken from a total of 500 states, starting from an initial state, ($350 < t_q \leq 500$). The need to introduce PIBDs is based on the fact that interesting creative patterns appear at intermediate states of system's evolution. PIBDs can also be used to evaluate the character of intermediate dynamic states and to compare them with the asymptotic behavior revealed by classic BDs.

3. Results

Without losing options, we present here the discrete time-space-distributed concentrations of the first constituent $X_1^{t_q}(R_p, R_s)$. The resulting sequences of space-distributed concentrations (images) are presented on squared lattices composed of 100×100 cells ($R_p, R_s = 1, 2, \ldots, 100$).

As an example, let us consider the evolution of the space-distributed concentrations $X_1^{t_q}(R_p, R_s)$ calculated with the genetic algorithm [Gontar & Grechko, 2006] set of parameters resulting in the sequence of symmetrical images at discrete time $t_q (q = 1, 2, \ldots, 10000, b = 0.44, k_1 = 7.32, k_2 = 7.34, \alpha_1 = -2.80, \alpha_2 = -3.73, \alpha_3 = -7.54, \beta_1 = 1.36, \beta_2 = -2.43, \beta_3 = 10.00)$. Four images taken from this sequence (at $q = 400, 450, 500, 10000$) are presented in Fig. 1(a).

Figure 1(b) shows four discrete time series $X_1^{t_q}(R_p^*, R_s^*)$ ($q = 350, 351, \ldots, 500$) taken from four arbitrarily chosen cells with coordinates $R_p^* = 1$, $R_s^* = 1$; $R_p^* = 4$, $R_s^* = 20$; $R_p^* = 25$, $R_s^* = 25$ and $R_p^* = 50$, $R_s^* = 50$. These time series corresponded to the sequence of 151 images [three of which are presented in Fig. 1(a)]. Discrete time evolutions of the concentrations in individual cells of the lattice have different character of their oscillatory regimes: the time series corresponding to the cell with coordinates $R_p^* = 1$, $R_s^* = 1$ is periodic (confirmed by the estimated Lyapunov exponent $\lambda < 0$), while the time series corresponding to the other three cells are chaotic (confirmed by the estimated Lyapunov exponents $\lambda > 0$). From the example presented here, one can suppose that the chaotic character of a local time series is somehow related to the appearance of the global complex patterns.

To illustrate the dynamics of the extracted time series, relevant to the patterns generated, we use partial intermediate bifurcation diagrams (PIBDs). Two examples of PIBDs ($350 < q \leq 500$) for $X_1^{t_q}(50, 50)$ versus b ($0.1 \leq b \leq 0.6$), and for $X_1^{t_q}(50, 50)$ versus α_1 ($-2.8 \leq \alpha_1 \leq -2.3$), are shown in Fig. 1(c). In Fig. 1(d) we show examples of images corresponding to the different values of parameter α_1 ($\alpha_1 = -2.4, \alpha_1 = -2.6, \alpha_1 = -2.656, \alpha_1 = -2.7$) calculated for $q = 500$. As can be seen in Fig. 1(d), complex patterns exist for α_1 corresponding to the parts of the PIBDs where the time series are chaotic ($\alpha_1 = -2.656, \alpha_1 = -2.7$), but not for α_1 corresponding to the periodic parts of the PIBDs ($\alpha_1 = -2.4, \alpha_1 = -2.6$).

To compare the asymptotic behavior of the considered time series to the intermediate regimes, classic partial bifurcation diagrams (BDs) have been calculated. Two examples of classic partial BDs ($9850 < q \leq 10000$) for $X_1^{t_q}(50, 50)$ versus $b (0.1 \leq b \leq 0.6)$, and for $X_1^{t_q}(50, 50)$ versus $\alpha_1 (-2.8 \leq \alpha_1 \leq -2.3)$, are presented in Fig. 1(e). In this particular example, we see that PIBDs and classic BDs demonstrate the same type of time series dynamics for the chosen parameters: transition to chaos via a cascade of period doubling.

It is interesting to compare the long-time behavior of the images' evolution to the corresponding images time series presented in BDs. For such purpose, in Fig. 1(f) we present images calculated at $q = 10000$, for the same parameters as used for the images presented in Fig. 1(d). The images corresponding to the periodic parts of BDs ($\alpha_1 = -2.4, \alpha_1 = -2.6$) converge into images that do not contain complex patterns, while the images corresponding to the chaotic parts of BDs ($\alpha_1 = -2.656, \alpha_1 = -2.7$) converge into complex

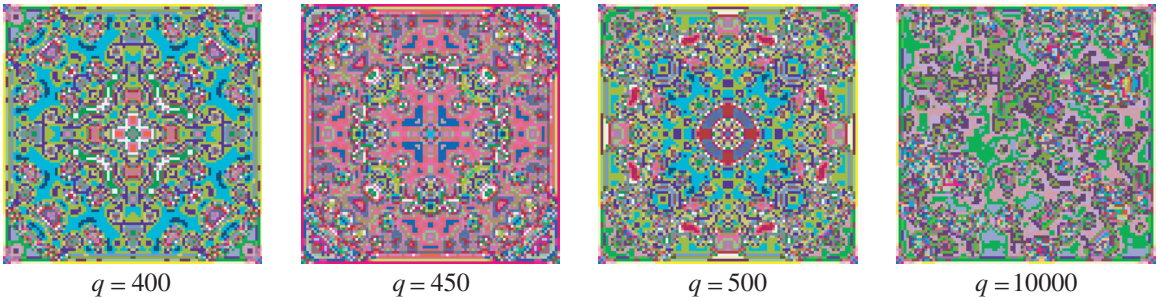

(a)

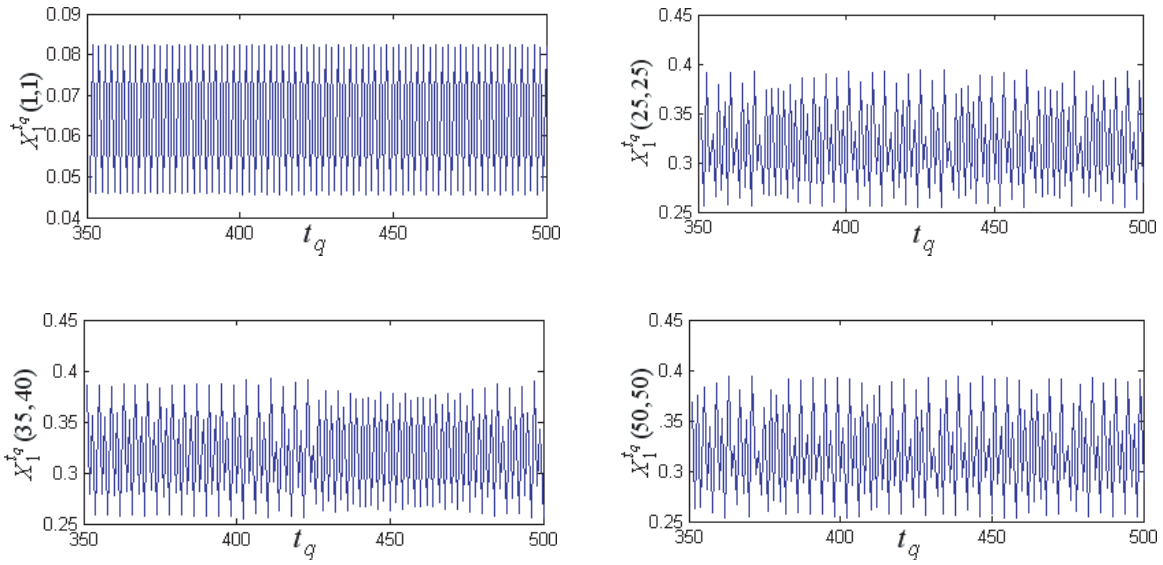

(b)

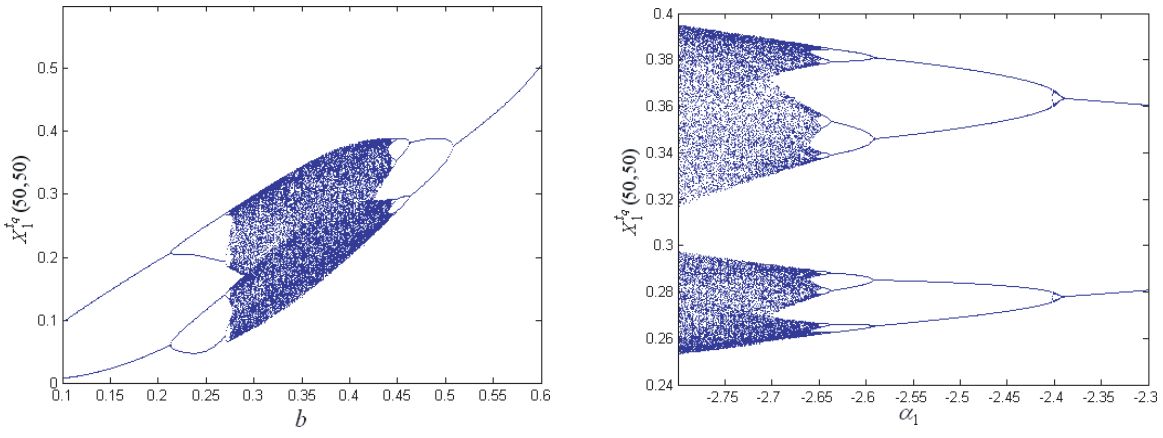

(c)

Fig. 1. (a) Four images of $X_1^{t_q}(R_p, R_s)(q = 400, 450, 500, 10000)$ calculated with the parameters: $b = 0.44$, $k_1 = 7.32$, $k_2 = 7.34$, $\alpha_1 = -2.80$, $\alpha_2 = -3.73$, $\alpha_3 = -7.54$, $\beta_1 = 1.36$, $\beta_2 = -2.43$, $\beta_3 = 10.00$. (b) Four local discrete time series: $X_1^{t_q}(1,1)$, $X_1^{t_q}(25,25)$, $X_1^{t_q}(35,40)$, $X_1^{t_q}(50,50)$ versus t_q $(q = 350, 351, \ldots, 500)$. (c) Two examples of PIBDs $(350 < q \leq 500)$ for $X_1^{t_q}(50,50)$ versus $b(0.1 \leq b \leq 0.6)$ and for $X_1^{t_q}(50,50)$ versus α_1 $(-2.8 \leq \alpha_1 \leq -2.3)$. (d) Four images corresponding to different values of parameter α_1 calculated at $q = 500$. (e) Two examples of BDs $(9850 < q \leq 10000)$ for $X_1^{t_q}(50,50)$ versus b $(0.1 \leq b \leq 0.6)$ and for $X_1^{t_q}(50,50)$ versus α_1 $(-2.8 \leq \alpha_1 \leq -2.3)$. (f) Four images corresponding to different values of parameter α_1 calculated at $q = 10000$.

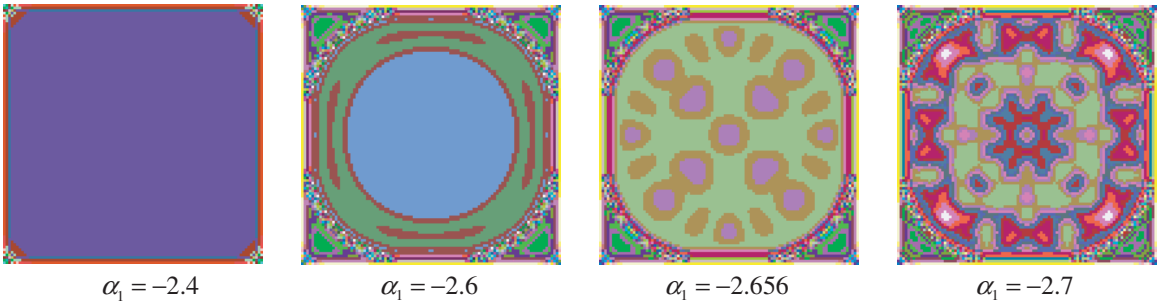

(d)

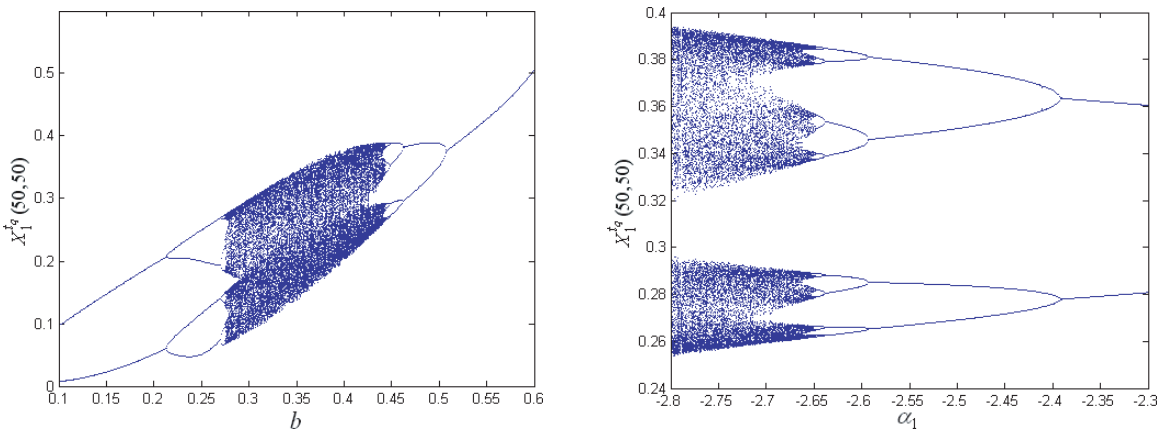

(e)

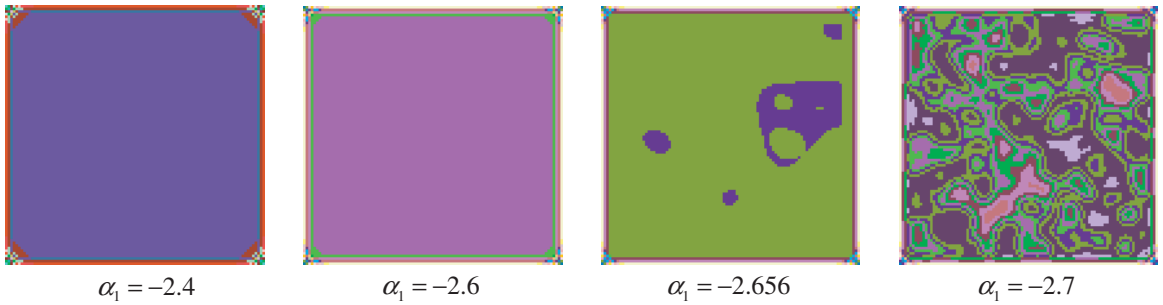

(f)

Fig. 1. (*Continued*)

patterns. As can be seen, the complex patterns at $q = 10000$ [Fig. 1(f)] have drastically changed their forms in comparison with the complex patterns at $q = 500$ [Fig. 1(d)]. This means that, in spite of the similar characters of PIBDs and classic BDs, embedded chaotic time series are different. This difference becomes apparent through the corresponding images. Therefore, by observing the evolution of the images, one can assess the changes in character of these images interrelated with chaotic signals.

The two following examples, presented in Figs. 2 and 3, illustrate and confirm our hypothesis concerning the necessity of the existence of chaotic regimes for complex discrete time space patterning. For this purpose, we have performed calculations with another two sets of parameters for generating images and time series: the first, $b = 9.01$, $k_1 = 8.38$, $k_2 = 1.91$, $\alpha_1 = -5.195$, $\alpha_2 = 2.29$, $\alpha_3 = 4.34$, $\beta_1 = 0.60$, $\beta_2 = -0.44$, $\beta_3 = 0.89$ (Fig. 2) and the second, $b = 0.14$, $k_1 = 9.24$, $k_2 = 2.77$, $\alpha_1 = 6.80$, $\alpha_2 = 6.00$, $\alpha_3 = -6.78$, $\beta_1 = -6.07$, $\beta_2 = 5.85$, $\beta_3 = 1.00$ (Fig. 3). As can be seen in Figs. 2 and 3, parameter changes resulted in different images and correspondingly different time series. The bifurcation

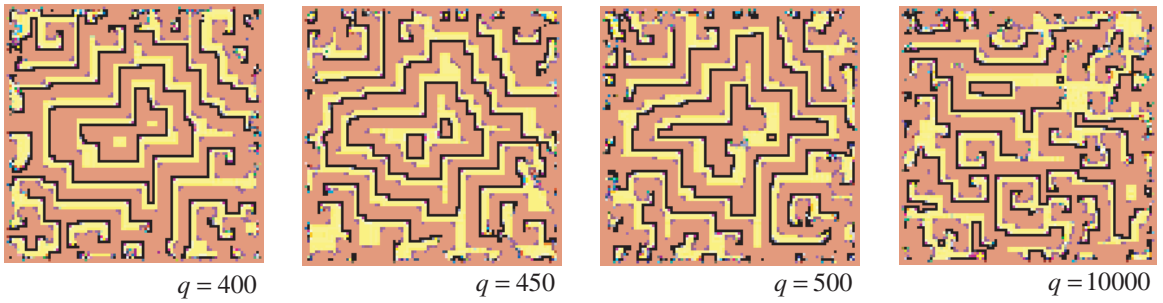

(a)

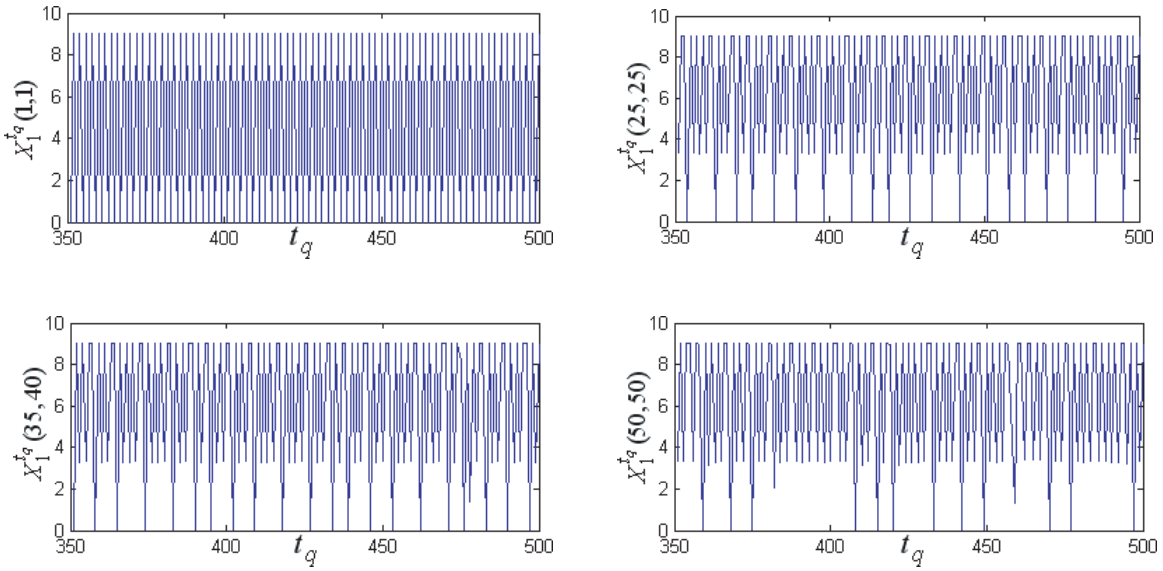

(b)

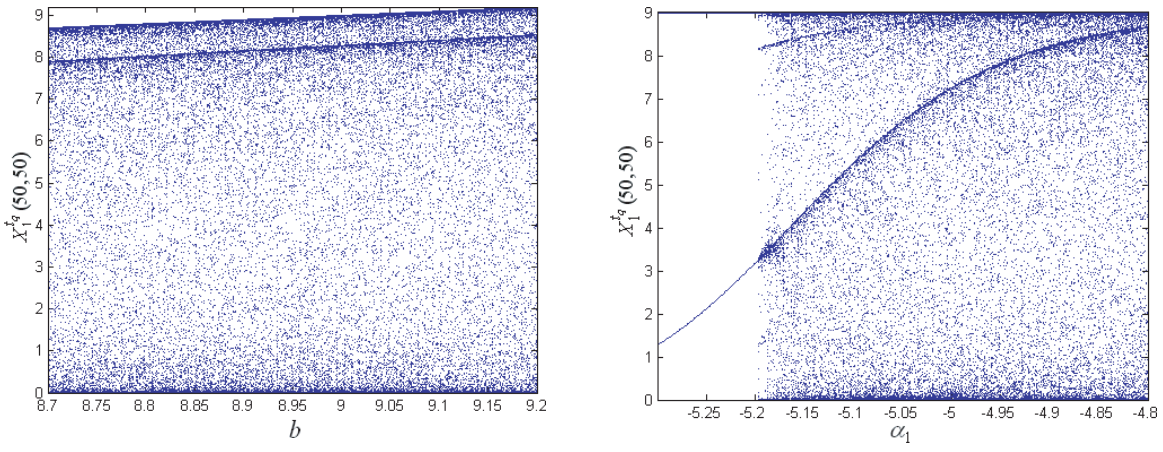

(c)

Fig. 2. (a) Four images of $X_1^{t_q}(R_p, R_s)(q = 400, 450, 500, 10000)$ calculated with the parameters: $b = 9.01$, $k_1 = 8.38$, $k_2 = 1.91$, $\alpha_1 = -5.195$, $\alpha_2 = 2.29$, $\alpha_3 = 4.34$, $\beta_1 = 0.60$, $\beta_2 = -0.44$, $\beta_3 = 0.89$. (b) Four local discrete time series: $X_1^{t_q}(1,1)$, $X_1^{t_q}(25,25)$, $X_1^{t_q}(35,40)$, $X_1^{t_q}(50,50)$ versus $t_q(q = 350, 351, \ldots, 500)$. (c) Two examples of PIBDs $(350 < q \leq 500)$ for $X_1^{t_q}(50,50)$ versus $b(8.7 \leq b \leq 9.2)$ and for $X_1^{t_q}(50,50)$ versus α_1 $(-5.3 \leq \alpha_1 \leq -4.8)$. (d) Four images corresponding to different values of parameter α_1 calculated at $q = 500$. (e) Two examples of BDs $(9850 < q \leq 10000)$ for $X_1^{t_q}(50,50)$ versus $b(8.7 \leq b \leq 9.2)$ and for $X_1^{t_q}(50,50)$ versus $\alpha_1(-5.3 \leq \alpha_1 \leq -4.8)$. (f) Four images corresponding to different values of parameter α_1 calculated at $q = 10000$.

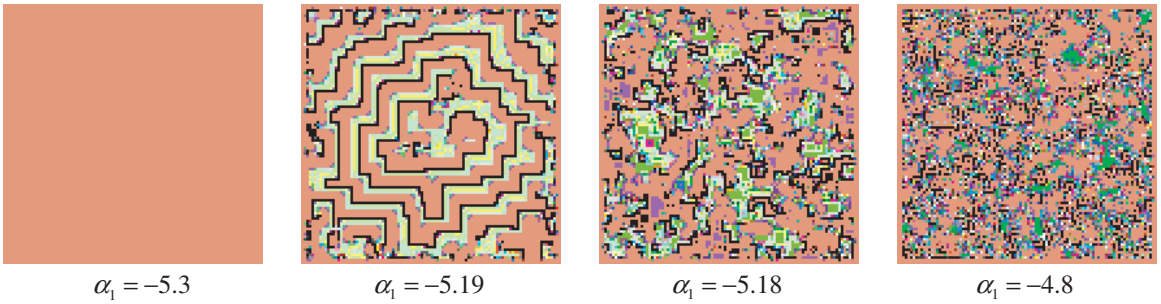

(d)

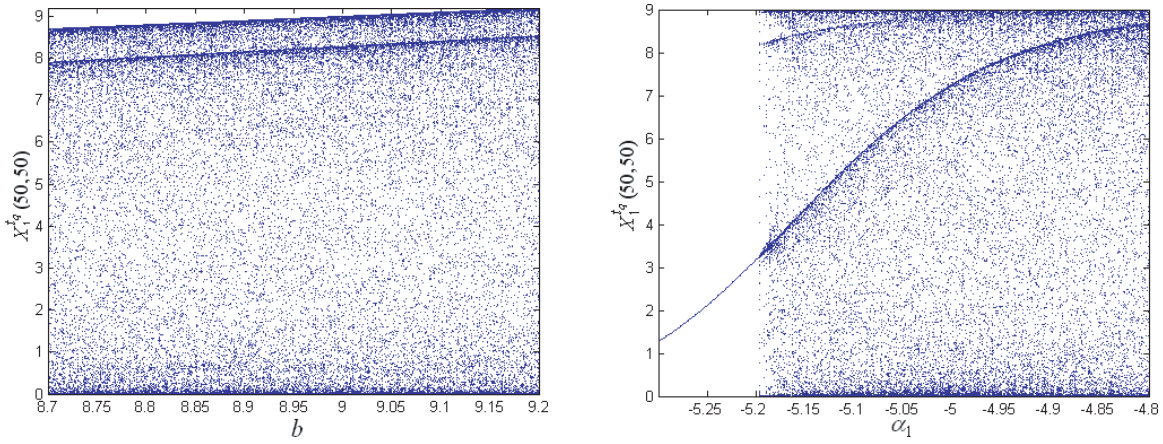

(e)

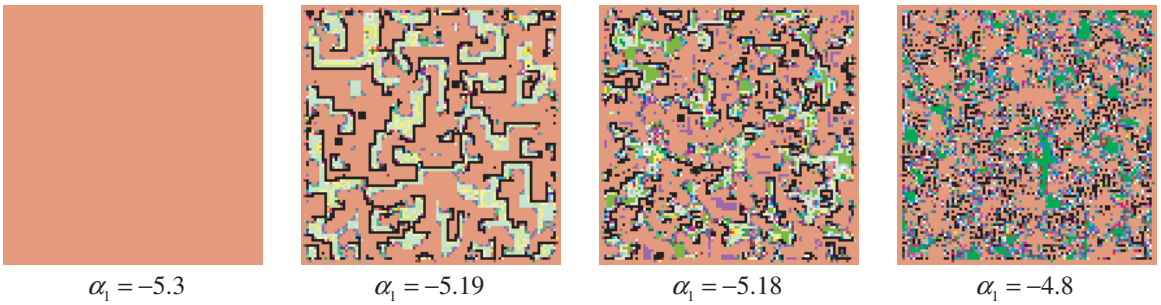

(f)

Fig. 2. (*Continued*)

diagrams also demonstrated different, from those presented earlier, scenarios of transition to chaos. These examples confirm our hypothesis about the existence of complex patterns only for the parameters taken from the chaotic parts of partial bifurcation diagrams. However, here we have presented bifurcation diagrams for the cell with coordinates $R_p^* = 50$, $R_s^* = 50$, the BDs for time series, taken from the other cells of the lattice, also have been calculated. For each set of parameters, BDs taken from the different cells have scenarios of the transition to chaos similar to that demonstrated by the corresponding BD from the cell with $R_p^* = 50$, $R_s^* = 50$.

As can be seen, presented here chaotic time series have different shapes and therefore can be considered to be informative signals reflecting complex chemical transformations accomplished with the interactions with the neighboring cells ("information exchange"). These interactions resulted in organization of the discrete time-space distributions of the constituents in the form of complex patterns.

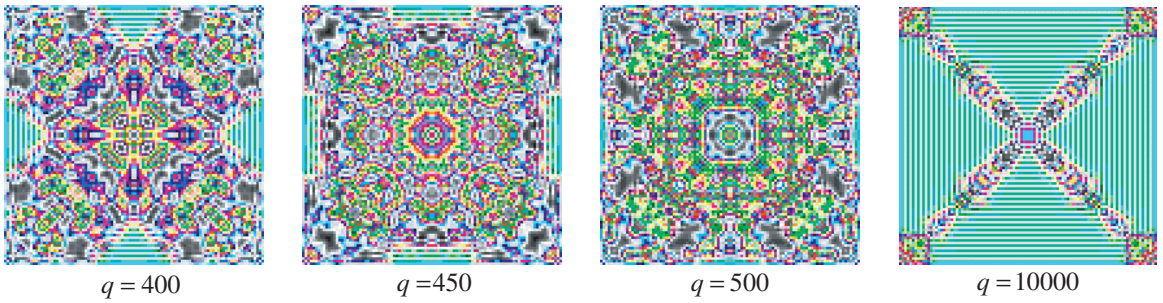

(a)

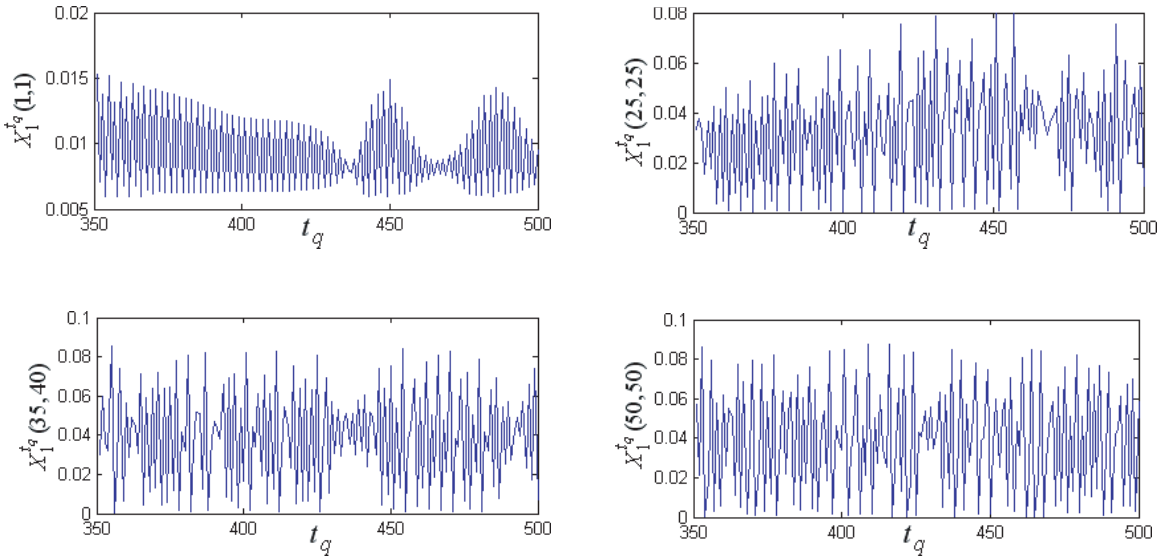

(b)

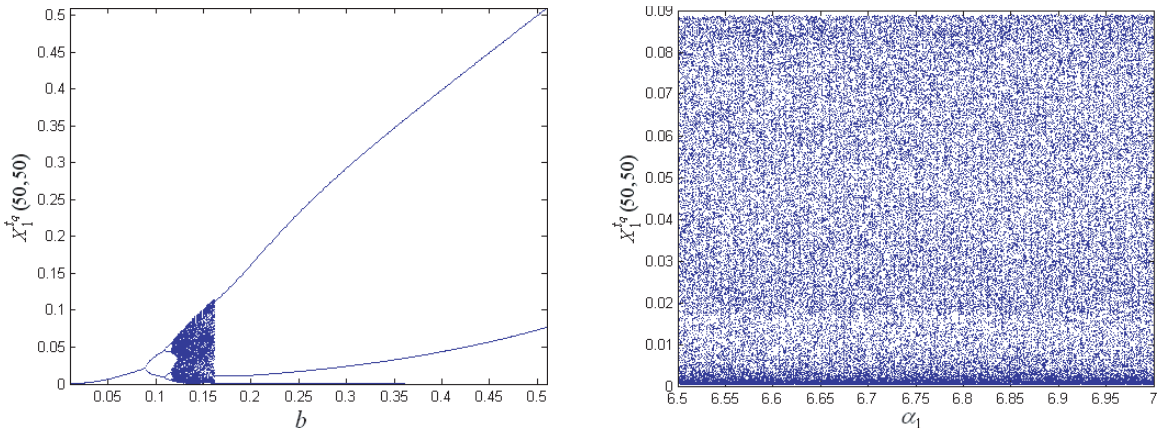

(c)

Fig. 3. (a) Four images of $X_1^{t_q}(R_p, R_s)(q = 400, 450, 500, 10000)$ calculated with the parameters: $b = 0.14$, $k_1 = 9.24$, $k_2 = 2.77$, $\alpha_1 = 6.80$, $\alpha_2 = 6.00$, $\alpha_3 = -6.78$, $\beta_1 = -6.07$, $\beta_2 = 5.85$, $\beta_3 = 1.00$. (b) Four local discrete time series: $X_1^{t_q}(1,1)$, $X_1^{t_q}(25,25)$, $X_1^{t_q}(35,40)$, $X_1^{t_q}(50,50)$ versus $t_q(q = 350, 351, \ldots, 500)$. (c) Two examples of PIBDs $(350 < q \leq 500)$ for $X_1^{t_q}(50,50)$ versus $b(0.001 \leq b \leq 0.5)$ and for $X_1^{t_q}(50,50)$ versus $\alpha_1(6.5 \leq \alpha_1 \leq 7)$. (d) Four images corresponding to different values of parameter α_1 calculated at $q = 500$. (e) Two examples of BDs $(9850 < q \leq 10000)$ for $X_1^{t_q}(50,50)$ versus $b(0.001 \leq b \leq 0.5)$ and for $X_1^{t_q}(50,50)$ versus $\alpha_1(6.5 \leq \alpha_1 \leq 7)$. (f) Four images corresponding to different values of parameter α_1 calculated at $q = 10000$.

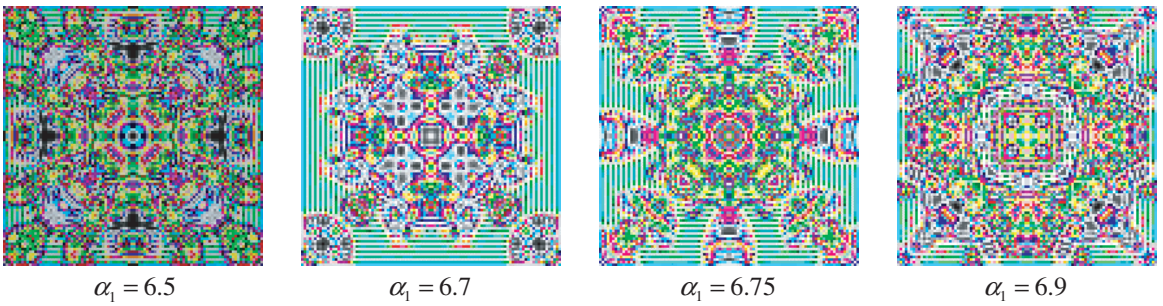

(d)

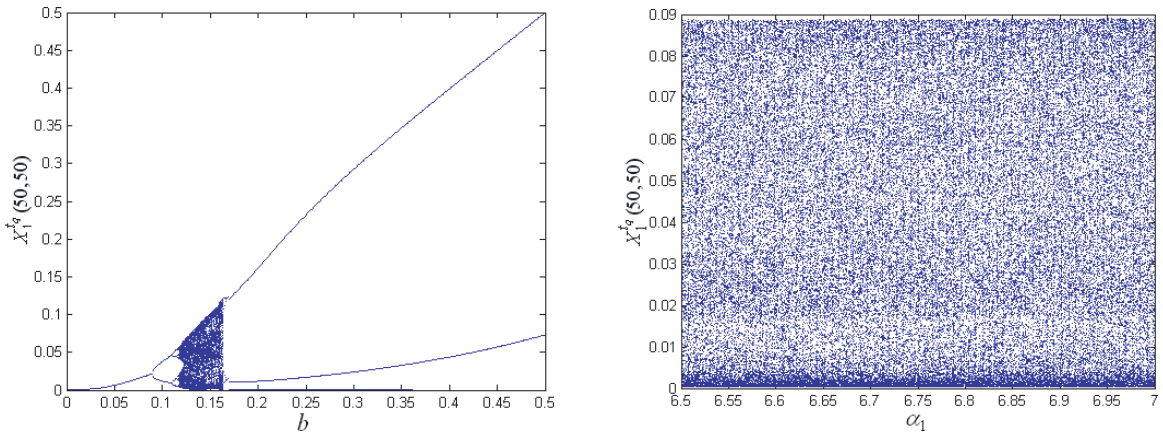

(e)

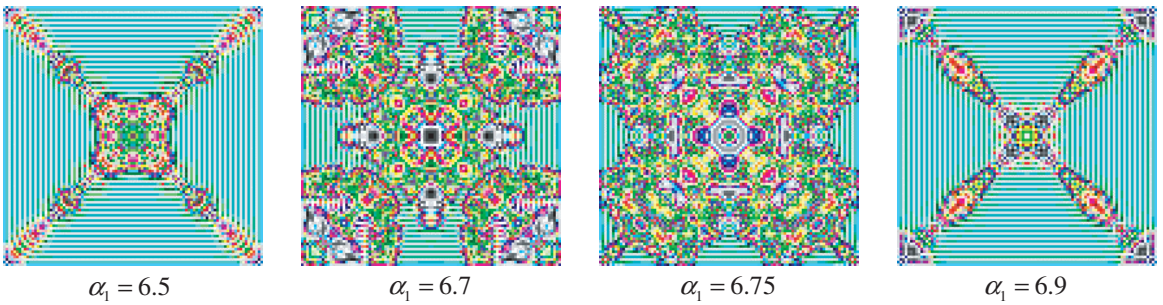

(f)

Fig. 3. (*Continued*)

4. Conclusions

The mathematical model presented here has demonstrated its ability to generate complex signals and images with some special features reflecting complex interrelations between local discrete time series and corresponding time-space distributed patterns. Analysis of the dynamic properties of the generated images and signals confirm the hypothesis that chaotic regimes play a crucial role in the emergence of complex creative patterns, e.g. ornaments, spirals, circles, etc. It was shown that the system of discrete lattice distributed difference Eqs. (1)–(3) with the embedded complex oscillatory regimes could provide coexisting periodic and chaotic time series with space distributed pattern's evolution and discrete space self-organization in the form of specific patterns and images. Therefore, these difference equations can be considered as a candidate for the development of "calculus of iterations" which can become additional to the calculus of infinitesimal mathematical

tool for complex systems dynamics mathematical modeling.

The results presented here can be used for mathematical modeling and visualization of complex physicochemical processes, complex biochemical reactions that take place in brain's neurons and in living cells networks, for constructing of artificial life and brain systems. Further studies of the mathematical model presented here should be directed to establishing functional relationship of the model's parameters and desired or experimentally observed dynamics of complex patterns and signals.

References

Gontar, V. [1997] "Theoretical foundation for the discrete chaotic dynamics of physicochemical systems: Chaos, self-organization, time and space in complex systems," *Discr. Dyn. Nature Soc.* **1**, 31–44.

Gontar, V. [2000] "Entropy as a driving force for complex and living systems dynamics," *Chaos Fract. Solit.* **11**, 231–236.

Gontar, V. [2004] "The dynamics of living and thinking systems, biological networks and the laws of physics," *Discr. Dyn. Nature Soc.* **8**, 101–111.

Gontar, V. & Grechko, O. [2006] "Generation of symmetrical colored images via solution of the inverse problem of chemical reactions discrete chaotic dynamics," *Int. J. Bifurcation and Chaos* **16**, 1419–1434.

Mandelbrot, B. B. [2004] *Fractals and Chaos* (Springer, NY).

Peitgen, H., Jurgens, H. & Saupe, D. [2004] *Chaos and Fractals* (Springer-Verlag, NY).

Schuster, H. G. [1984] *Deterministic Chaos* (Physik-Verlag, Weinheim).